Phase Transitions in Epitaxial (−110) $BiFeO_3$ Films from First Principles

S. Prosandeev,[1,2] Igor A. Kornev,[3] and L. Bellaiche[1,2]

[1]*Physics Department, University of Arkansas, Fayetteville, Arkansas 72701, USA*
[2]*Institute for Nanoscience and Engineering, University of Arkansas, Fayetteville, Arkansas 72701, USA*
[3]*Laboratoire Structures, Propriétés et Modélisation des Solides, Ecole Centrale Paris, CNRS-UMR8580, Grande Voie des Vignes, 92295 Châtenay-Malabry Cedex, France*

(Received 10 May 2011; published 8 September 2011)

The effect of misfit strain on properties of epitaxial $BiFeO_3$ films that are grown along the pseudocubic $[\bar{1}10]$ direction, rather than along the usual [001] direction, is predicted from density-functional theory. These films adopt the monoclinic *Cc* space group for compressive misfit strains smaller in magnitude than $\simeq 1.6\%$ and for any investigated tensile strain. In this *Cc* phase, both polarization and the axis about which antiphase oxygen octahedra tilt rotate within the epitaxial plane as the strain varies. Surprisingly and unlike in (001) films, for compressive strain larger in magnitude than $\simeq 1.6\%$, the polarization vanishes and two orthorhombic phases of *Pnma* and $P2_12_12_1$ symmetry successively emerge via strain-induced transitions. The *Pnma*-to-$P2_12_12_1$ transition is a rare example of a so-called pure gyrotropic phase transition, and the $P2_12_12_1$ phase exhibits original interpenetrated arrays of ferroelectric vortices and antivortices.

DOI: 10.1103/PhysRevLett.107.117602 PACS numbers: 77.55.Nv, 61.50.Ah, 71.15.Mb, 77.80.bn

Multiferroic $BiFeO_3$ (BFO) materials have been experiencing a huge resurgence of interest in the last 8 years or so, mostly because they exhibit coupled long-range-ordered electric and magnetic degrees of freedom at room temperature (see, e.g., Ref. [1]). In particular, recent striking features have been reported in epitaxial $BiFeO_3$ thin films. Examples include a strain-driven phase transition towards states with giant axial ratio and large out-of-plane polarization [2–5], dramatic enhancement of magnetoelectric coefficients near this phase transition [6,7], and the possibility of generating large piezoelectric responses because of the coexistence of nanodomains made of different phases [8]. Other examples are the strong and counterintuitive dependency of critical transition temperatures with the epitaxial strain [9], and the prediction of array of ferroelectric vortices [10] that was then experimentally confirmed [11]. Interestingly, all these latter breakthroughs were reported for (001) $BiFeO_3$ thin films. On the other hand, very little is known about BFO films that are grown along directions that are different from the usual pseudocubic [001] direction [12–14]. It is therefore legitimate to wonder if further surprises are in store when playing with the growth direction in BFO, especially when realizing that such fascinating material exhibits many different metastable states in its bulk form [15].

The aim of this Letter is to investigate the effect of compressive and tensile strains on properties of epitaxial BFO films that are grown along the pseudocubic $[\bar{1}10]$ direction, by performing 0 K first-principle calculations. As we will see, surprises are indeed in store. For instance, the equilibrium ground-state for tensile strain and small compressive strain is found to be of monoclinic *Cc* symmetry and possesses two order parameters that both fully lie within the $(\bar{1}10)$ epitaxial plane and rotate within that plane when the strain is varied. These parameters are the polarization and a vector quantifying both the axis about which the oxygen octahedra tilt in antiphase fashion and the magnitude of such tilting. Furthermore, for compressive strain ranging between $\simeq -1.6\%$ and $\simeq -7\%$, the *Cc* state is destabilized via a phase transition in favor of a nonpolar orthorhombic phase of *Pnma* symmetry. Such latter phase is characterized by both in-phase and out-of-phase oxygen octahedra tiltings and by additional antiphase Bi displacements associated with the *X* point of the first Brillouin zone [15]. For even larger-in-magnitude compressive strain, a novel paraelectric phase of $P2_12_12_1$ space group becomes the ground-state via another phase transition. Such phase possesses an additional order parameter with respect to *Pnma*, that is antiphase Bi displacements associated with the *M* point of the first Brillouin zone. This unusual coexistence of several order parameters leads to the original formation of interpenetrated arrays of ferroelectric vortices and antivortices in the $P2_12_12_1$ state. Furthermore, the *Pnma*-to-$P2_12_12_1$ transition constitutes a rare example [16] of a so-called gyrotropic phase transition (that is characterized by the appearance of a spontaneous optical activity) [17–20]. In fact, to the best of our knowledge, this study reports the first pure gyrotropic phase transition ever predicted or observed in a perovskite material.

Here, we perform density-functional calculations (DFT) at 0 K [21] using the Vienna *ab initio* simulation package (VASP) [22] within the local spin density approximation plus the Hubbard parameter *U* (LSDA + *U*) with $U = 3.87$ eV [23,24]. We use the projected augmented wave (PAW) method and a $3 \times 2 \times 3$ *k* point mesh and an energy cutoff of 500 eV. We employ a 20-atom cell, in which a *G*-type antiferromagnetic order is assumed. In

order to mimic a perfect epitaxy on a (−110) plane, the lattice vectors of this 20 atom unit cell are given, in the Cartesian (x', y', z') setting for which the x', y', and z' axes are along the pseudocubic [001], [110], and [$\bar{1}$10] directions, respectively, by $\mathbf{a_1} = a(\delta_1, \delta_2, \sqrt{2} + \delta_3)$, $\mathbf{a_2} = a(2, 0, 0)$ and $\mathbf{a_3} = a(0, \sqrt{2}, 0)$, where a is the lattice constant of the substrate. The $\mathbf{a_2}$ and $\mathbf{a_3}$ lattice vectors are thus along the pseudocubic [001] and [110] directions, respectively, and therefore both belong to the ($\bar{1}$10) plane—unlike the $\mathbf{a_1}$ vector. The misfit strain (to be denoted by η_{mis} in the following) is defined as $(a - a_0)/a_0$, where a_0 corresponds to the pseudocubic 0 K lattice parameter of BFO bulk (which is equal to 3.9 Å in our case). For each considered value of a, the δ_1, δ_2 and δ_3 variables and internal atomic coordinates are relaxed to minimize the total energy, Hellman-Feynman forces and the σ_3, σ_4 and σ_5 components of the stress tensor in the (x', y', z') setting. Note that $1 + \frac{\delta_3}{\sqrt{2}}$ is the axial ratio.

For each in-plane lattice constant, a, we focus on the phases that have the lowest total energy. Figure 1 reports the energy of these phases as a function of the misfit strain, with this latter varying between −9% and +9%. In addition to the axial ratio, Figs. 2 and 3 show the evolution of five physical vectors (in the equilibrium phases) as a function of misfit strain, in two different frames: in the (x', y', z') Cartesian basis indicated above for which the z'-axis coincides with the out-of-plane direction, and in the (x, y, z) Cartesian basis for which the x, y, and z axes are along the pseudocubic [100], [010], and [001] directions, respectively. Three of these vectors are: (i) the polarization, $\mathbf{P}$, that is evaluated from the product of the atomic displacements with the Born effective charges;

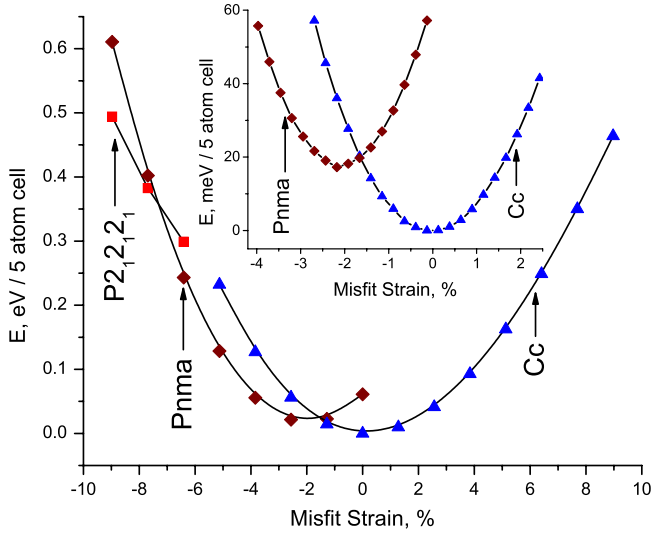

FIG. 1 (color online). Total energy versus misfit strain for the equilibrium phases in an epitaxial (−110) BFO film, as computed from LSDA + U calculations in a 20-atom cell. The inset displays the same information but for a narrower range of misfit strain ranging from ≃ −4% to ≃ +2%.

(ii) the $\boldsymbol{\omega}_\mathbf{R}$ vector whose direction is the axis about which the antiphase oxygen octahedra associated with the R point of the 5-atom first Brillouin zone tilt while its magnitude is the angle of such tilting [24]; and (iii) the $\boldsymbol{\omega}_\mathbf{M}$ vector that characterizes the direction and strength of the in-phase oxygen octahedra tilting associated with the M point of the 5-atom first Brillouin zone (here, this M point corresponds to $\pi/a(1, 1, 0)$ in the (x, y, z) frame). The remaining two other vectors, $\mathbf{g_X}$ and $\mathbf{g_M}$, are defined such as their α-Cartesian components are given by

$$g_{X,\alpha} = \frac{1}{V}\sum_j Z^*_{Bi,\alpha\alpha}\,\delta r^{Bi}_{j,\alpha}\, e^{i\mathbf{k_X}.\mathbf{R_j}}$$
$$g_{M,\alpha} = \frac{1}{V}\sum_j Z^*_{Bi,\alpha\alpha}\,\delta r^{Bi}_{j,\alpha}\, e^{i\mathbf{k_M}.\mathbf{R_j}}, \quad (1)$$

where $\mathbf{R_j}$ locates the center of the jth 5-atom cell, and $\delta r^{Bi}_{j,\alpha}$ is the α-component of the displacement of the Bi atom in the jth 5-atom cell (with respect to a

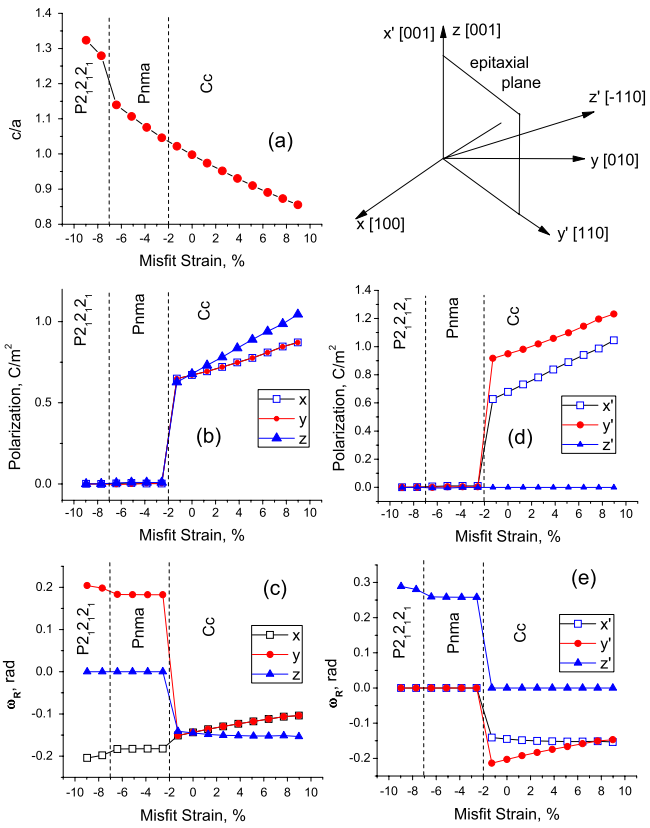

FIG. 2 (color online). Predicted physical properties of an epitaxial (−110) BFO film versus the misfit strain in the equilibrium phases. Panels (a) shows the axial ratio. Panels (b) and (c) display the Cartesian components of the polarization and $\boldsymbol{\omega}_\mathbf{R}$ antiferrodistortive vector associated with the R point in the (x, y, z) frame, respectively. Panels (d) and (e) show similar data than Panels (b) and (c) but in the (x', y', z') frame for which the z' axis is along the out-of-plane direction. The top right schematizes the two frames.

centrosymmetric configuration). $\mathbf{k_X}$ is the X point of the first Brillouin zone of the 5-atom cell that corresponds to $\pi/a(0, 0, 1)$ in the (x, y, z) frame, while $\mathbf{k_M}$ is the M point of the first Brillouin zone associated with 5-atom cells and corresponding to $\pi/a(1, 1, 0)$ in the (x, y, z) frame. Finally, Z^*_{Bi} is the effective charge tensor of Bi atoms and V is the supercell volume. The sums run over all the 5-atom cells j belonging to the supercell. $\mathbf{g_X}$ and $\mathbf{g_M}$ thus quantify specific antiphase displacements of the Bi atoms.

Figure 1 reveals the existence of three different equilibrium phases within the misfit strain region considered here. Their space group is determined from the "FINDSYM" [25] and "BPLOT" [26] programs. The first phase has a monoclinic Cc symmetry and is the lowest-in-energy state for η_{mis} ranging between $\simeq -1.6\%$ and $+9\%$. Note that Cc phases have been previously found in (001) BFO films [4–7]. Interestingly, Figs. 2 indicate that the present Cc state is characterized, at zero misfit strain, by a polarization lying along the in-plane pseudocubic [111] direction and by antiphase oxygen octahedra (associated with the R point of the first Brillouin zone) tilting about the same axis. As the strain progressively increases towards $+9\%$, the polarization increases in magnitude and rotates towards the pseudocubic [334] direction, while always staying within the epitaxial (-110) plane. During this evolution, the overall oxygen octahedra tilts become weaker while their axis also rotate within the epitaxial plane (towards the [223] pseudocubic direction) [27]. Figure 2(a) also shows that the axial ratio progressively decreases from 1.02 to 0.86 as η_{mis} varies between $\simeq -1.5\%$ and $+9\%$. Interestingly, a recent experimental study [14] investigated (110) BFO thin films that were grown on a (110) $SrTiO_3$ substrate but that were partially relaxed, which led to an average misfit strain $\simeq -0.5\%$. Such films were found to exhibit a monoclinic phase and a value of $\simeq 1.02$ for the axial ratio we defined above, which agree well with our predictions.

One major finding of this study is that the Cc state becomes metastable for compressive strain lower than $\simeq -1.6\%$, in favor of a new phase having the orthorhombic $Pnma$ space group. This $Pnma$ phase has no polarization at all [see Figs. 2(b) and 2(d)]. As a result, the presently discovered Cc-to-$Pnma$ transition under compressive strain in (-110) BFO films is a ferroelectric-to-paraelectric transition. This contrasts with the so-called R-to-T transition occurring in (001) BFO films under compressive strain and that concerns two polar states [3,8]. In fact, the $Pnma$ phase is characterized by (i) oxygen octahedra tilting in antiphase manner about the pseudocubic, out-of-plane $[\bar{1}10]$ direction [see Figs. 2(c) and 2(e)]; (ii) oxygen octahedra tilting in-phase about the pseudocubic, in-plane [001] direction [see Figs. 3(a) and 3(d)]; and (iii) antiphase, out-of-plane Bi-displacements that correspond to a $\mathbf{g_X}$-vector oriented along the $[1\bar{1}0]$ direction [see Figs. 3(b) and 3(e)]. Interestingly, $Pnma$ exists in BFO bulk [28] at high temperature, but is a metastable state in (rather than the ground state of) BFO bulk at low temperature [15]—unless one applies high enough pressure [29]. Note that the presently discovered $Pnma$ state has its energy minimum being higher than the minimum of the Cc state by only $\simeq$20 meV per 5 atom, which is of the same order than the predicted difference in minimum between the $R3c$ and $Pnma$ phases in bulk BFO at $T = 0$ K [15]. Interestingly, common substrates (such as $SrTiO_3$, $DyScO_3$, $(LaAlO_3)O_{0.3}$-$(Sr_2AlTaO_6)_{0.7}$ and $GdScO_3$) fall in within the $-2.5\% - 0\%$ misfit strain region [9], which should make the observation of the predicted $Pnma$ and Cc phases feasible.

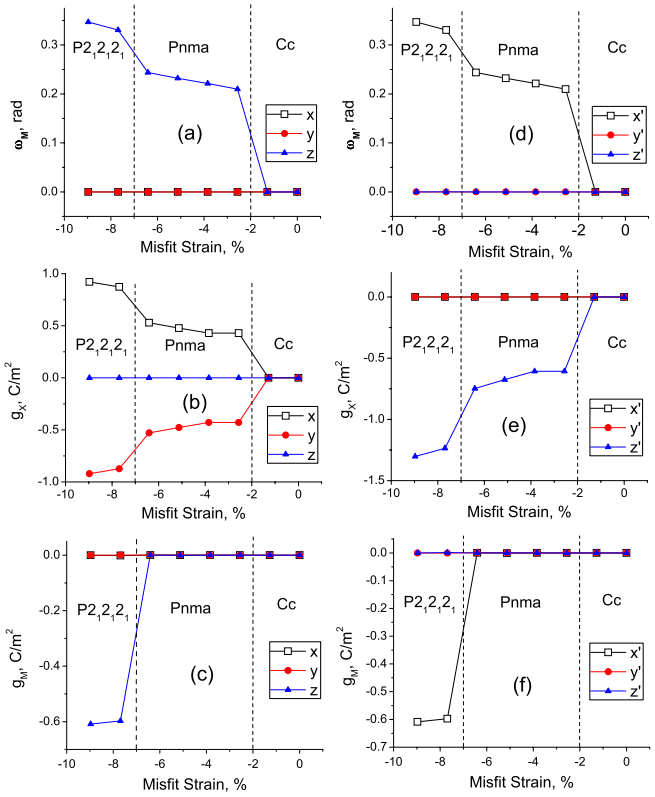

FIG. 3 (color online). Other predicted physical properties of an epitaxial (-110) BFO film versus the misfit strain in the equilibrium phases. Panels (a),(b), and (c) display the Cartesian components of the order parameters $\omega_{\mathbf{M}}$, $\mathbf{g_X}$ and $\mathbf{g_M}$ (see text) in the (x, y, z) frame, respectively. Panels (d)–(f) show similar data than Panels (a)-(c) but in the (x', y', z') frame for which the z' axis is along the out-of-plane direction.

Figs. 2(c) and 2(e) also indicate that increasing the strength of the compressive strain within $Pnma$ does not affect the tilting of the oxygen octahedra associated with the R point. On the other hand, such increase enhances the in-phase tilting of the oxygen octahedra [see Figs. 3(a) and 3(d)] and the antiphase Bi displacements associated with the X point [see Figs. 3(b) and 3(e)], in addition to enlarge the axial ratio [cf. Fig. 2(a)].

Another striking feature of Fig. 1 is the destabilization of the *Pnma* state in favor of another phase that is still orthorhombic and still paraelectric, for compressive strain larger in magnitude than ≃7%. However, this new phase has a different space group, namely, is of $P2_12_12_1$ symmetry. It mostly differs from the *Pnma* by a giant axial ratio (of the order of 1.3) and by the activation of Bi antiphase displacements along the in-plane, pseudocubic [001] direction and that are associated with the *M* point [see Figs. 3(c) and 3(f) for the corresponding $\mathbf{g_M}$ order parameter]. Figs. 2 and 3 also indicate that the phase transition between *Pnma* and $P2_12_12_1$ results in an enhancement (but does not modify the direction) of $\omega_\mathbf{R}$, $\omega_\mathbf{M}$ and $\mathbf{g_X}$ [30]. Figs. 1–3 thus reveal that applying compressive strain in (−110) BFO films is dramatically different than applying compressive strain in (001) BFO films, in the sense that the former enhances oxygen octahedra tiltings and antiferroelectric displacements and opposes the formation of a polarization, while the latter leads to giant-polarization phases with small or vanishing antiferrodistortive and antiferroelectric motions [3–7]. Moreover and as shown in Fig. 4, the coexistence of these $\mathbf{g_X}$ and $\mathbf{g_M}$ parameters in the $P2_12_12_1$ state leads to the formation of interpenetrated arrays of ferroelectric vortices and antivortices. Interestingly, Fig. 4 further shows that all the vortices have exactly the same chirality, which is consistent with the fact that $P2_12_12_1$ phases are allowed to have nonzero optical activity tensors [20] and nonzero gyrotropic tensors [18]. In fact, the *Pnma*-to-$P2_12_12_1$ phase transitions fall in the category of the so-called gyrotropic phase transitions, that are characterized by the appearance of a spontaneous optical activity [16–20]. It is important to realize that gyrotropic phase transitions are rare in nature, especially when being of pure type (for which no polarization or no new components of the strain tensor emerge, as it is in the present case) [18]. In fact, we are not aware of any gyrotropic phase transition that has ever been reported in any perovskite. Note, however, that a coexistence of a *Pnma* state with a $P2_12_12$ phase has been experimentally detected in $(Sr_{1-x}Ca_x)TiO_3$ ceramics for some composition range [33]. It is interesting to realize that $P2_12_12$ is another orthorhombic and gyrotropic phase and that it shares the same point group than $P2_12_12_1$, that is 222. Moreover, while a *Pnma*-to-$P2_12_12_1$ gyrotropic phase transition has been previously observed in $(C_5H_{11}NH_3)_2ZnCl_4$ [16] and that the coexistence of nearby ferroelectric vortices and antivortices has been recently artificially created in $BiFeO_3$ films [34], no (spontaneous) interpenetrated arrays of these two kinds of topological defects have ever been predicted or seen in any material to the best of our knowledge [35]. Note also that we are not aware of any previous prediction or observation of a stable $P2_12_12_1$ phase in BFO systems, and that $YAlO_3$ (YAO) has a lattice constant that is around 7% smaller than that of $BiFeO_3$. In other words, growing BFO on a (110) YAO substrate should lead to the detection of the presently predicted $P2_12_12_1$ state [37]. This $P2_12_12_1$ phase is also likely to form for smaller-in-magnitude strain at finite temperature.

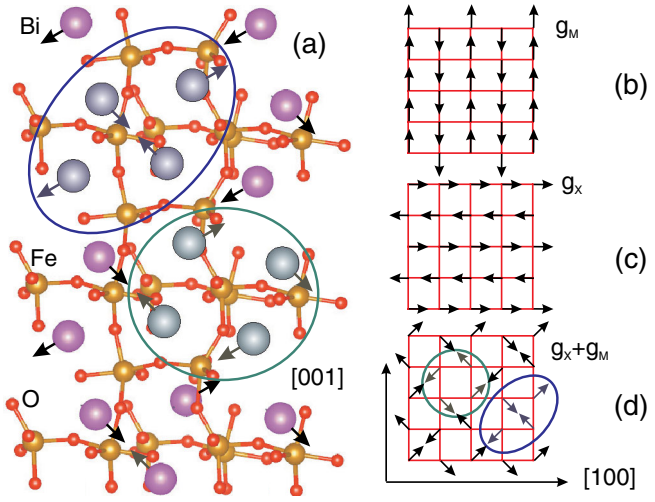

FIG. 4 (color online). Atomic features of the predicted $P2_12_12_1$ state. Panel (a) displays the crystallographic structure. Panels (b), (c) and (d) schematize the Bi displacements associated with the projection of $\mathbf{g_M}$, $\mathbf{g_X}$ and of the sum of these two latter order parameters, respectively, in a pseudocubic (010) plane. The green (respectively, blue) arrows/circles are used to emphasize a ferroelectric vortex (respectively, antivortex).

In summary, we have studied, from first-principles, properties of (−110) BFO films under epitaxial strain. Several striking features were found, including (i) a polar, monoclinic *Cc* state in which the polarization and the axis about which antiphase oxygen octehadra tilt are both in-plane and rotate within the epitaxial plane as the strain varies from ≃ −1.6% to +9%; (ii) a phase transition from *Cc* to a nonpolar orthorhombic *Pnma* state for a misfit strain around ≃ −1.6%; and (iii) a pure gyrotropic phase transition from this *Pnma* to a $P2_12_12_1$ phase possessing interpenetrated arrays of ferroelectric vortices and antivortices, for an epitaxial strain ≃ −7%. The possibility of observing the first gyrotropic phase transition in perovskites is also mentioned. We thus hope that our study is of large benefits to the active and fascinating research fields of multiferroics, nanoscience and phase transitions.

This work is mostly supported by ONR Grants N00014-08-1-0915, N00014-11-1-0384, and N00014-07-1-0825 (DURIP). We also acknowledge the Department of Energy, Office of Basic Energy Sciences, under contract ER-46612, and NSF grants DMR-0701558 and DMR-0080054 (C-SPIN). Some computations were made possible thanks to the MRI NSF grant 0722625 and to a Challenge grant from HPCMO of the U.S. Department of Defense.

[1] G. Catalan and J. F. Scott, Adv. Mater. **21**, 2463 (2009).
[2] H. Béa *et al.*, Phys. Rev. Lett. **102**, 217603 (2009).
[3] R. J. Zeches *et al.*, Science **326**, 977 (2009).
[4] A. J. Hatt, N. A. Spaldin, and C. Ederer, Phys. Rev. B **81**, 054109 (2010).
[5] B. Dupé *et al.*, Phys. Rev. B **81**, 144128 (2010).
[6] J. C. Wojdel and J. Íñiguez, Phys. Rev. Lett. **105**, 037208 (2010).
[7] S. Prosandeev, I. A. Kornev, and L. Bellaiche, Phys. Rev. B **83**, 020102(R) (2011).
[8] J. X. Zhang *et al.*, Nature Nanotech. **6**, 98 (2011).
[9] I. C. Infante *et al.*, Phys. Rev. Lett. **105**, 057601 (2010).
[10] S. Prosandeev, S. Lisenkov, and L. Bellaiche, Phys. Rev. Lett. **105**, 147603 (2010).
[11] C. T. Nelson *et al.*, Nano Lett. **11**, 828 (2011).
[12] H. W. Jang *et al.*, Phys. Rev. Lett. **101**, 107602 (2008).
[13] K. Sone *et al.*, Jpn. J. Appl. Phys. **49**, 09MB03 (2010).
[14] D. Kan and I. Takeuchi, J. Appl. Phys. **108**, 014104 (2010).
[15] O. Diéguez, O. E. Gonzalez-Vazquez, J. C. Wojdel and J. Íñiguez, Phys. Rev. B **83**, 094105 (2011).
[16] A. Gomez Cuevas *et al.*, Phys. Rev. B **29**, 2655 (1984).
[17] S. Hirotsu, J. Phys. C **8**, L12 (1975).
[18] C. Konak, V. Kopsky, and F. Smutny, J. Phys. C **11**, 2493 (1978).
[19] H. Wondratschek and W. Jeitschko, Acta Crystallogr. Sect. A **32**, 664 (1976).
[20] S. V. Akimov and E. F. Dudnik, Phys. Solid State **51**, 1420 (2009).
[21] W. Kohn and L. J. Sham, Phys. Rev. **140**, A1133 (1965).
[22] G. Kresse and J. Hafner, Phys. Rev. B **47**, 558 (1993); G. Kresse and J. Furthmüller, Phys. Rev. B **54**, 11 169 (1996).
[23] V. I. Anisimov, F. Aryasetiawan, and A. I. Lichtenstein, J. Phys. Condens. Matter **9**, 767 (1997).
[24] I. A. Kornev *et al.*, Phys. Rev. Lett. **99**, 227602 (2007).
[25] see http://stokes.byu.edu/findsym.html.
[26] see http://www.cryst.ehu.es/cryst/bplot.html.
[27] We also numerically found a stable phase that has a *Pc* space group and for which both **P** and the axis about which the oxygen octahedra tilt lie close to the $[1\bar{1}1]$ pseudocubic direction. In other words, this *Pc* state possesses a polarization and a $\omega_{\mathbf{R}}$ vector that both have an out-of-plane component in addition to an in-plane component. However, this *Pc* state has a higher energy than the present *Cc* phase for any considered strain, except for $\eta_{\text{mis}} = 0\%$ for which the two phases have the same energy.
[28] D. C. Arnold, K. S. Knight, F. D. Morrison, and P. Lightfoot, Phys. Rev. Lett. **102**, 027602 (2009); D. Kan *et al.*, Adv. Funct. Mater. **20**, 1108 (2010).
[29] R. Haumont *et al.*, Phys. Rev. B **79**, 184110 (2009).
[30] Note that the *Pnma*-to-$P2_12_12_1$ transition involves two nonpolar states, exactly as in (001) $SrTiO_3$ films under strain [31]. Note also that the present Letter emphasizes that films grown along directions that are different from (001) can exhibit rather surprising results, as consistent with Ref. [32] on $PbTiO_3$ films.
[31] N. A. Pertsev, A. K. Tagantsev, and N. Setter, Phys. Rev. B **61**, R825 (2000).
[32] A. K. Tagantsev, N. A. Pertsev, P. Muralt, and N. Setter, Phys. Rev. B **65**, 012104 (2001).
[33] S. Anwar and N. P. Lalla, J. Phys. Condens. Matter **19**, 436210 (2007).
[34] N. Balke *et al.*, Nature Nanotech. **4**, 868 (2009).
[35] Note, however, that complex topological defects have been predicted in arrays of thin $BaTiO_3$ nanowires [36]. Examples include radial defects, antivortices and even a topological defect that has a winding number of -3.
[36] J. Hong *et al.*, Phys. Rev. B **81**, 172101 (2010).
[37] Despite the large misfit strain between YAO and BFO, successful growth of BFO films on YAO has been demonstrated for (001) films [3], likely because BFO has so many degrees of freedom (polarization, antiferroelectric displacements, oxygen octahedra tiltings) that it can adapt to substrates with different lattice constants.